Fracture healing is delayed in the absence of gasdermin signaling

Kai Sun[1,2,3], Chun Wang[2], Jianqiu Xiao[2], Michael D. Brodt[4], Luorongxin Yuan[2], Tong Yang[1,2,3], Yael Alippe[2], Huimin Hu[3], Dingjun Hao[1,3], Yousef Abu-Amer[4,5], Matthew J. Silva[4], Jie Shen[4], Gabriel Mbalaviele[2*]

[1]Xi'an Jiaotong University Health Science Center, Xi'an, Shaanxi, China; [2]Division of Bone and Mineral Diseases, Washington University School of Medicine, St. Louis, MO 63110, USA; [3]Department of Spine Surgery, Honghui Hospital, Xi'an Jiaotong University, Xi'an, Shaanxi, China; [4]Department of Orthopaedic Surgery, Washington University School of Medicine, St. Louis, Missouri, USA; [5]Shriners Hospital for Children, St. Louis, Missouri, USA

Running title: Gasdermin signaling in fracture healing

[*]To whom correspondence should be addressed. Division of Bone and Mineral Diseases, Washington University School of Medicine, 660 South Euclid Avenue, Campus Box 8301, St. Louis, MO 63110, Phone: (314) 286-1114; Fax: (314) 454-5047; e-mail: gmbalaviele@wustl.edu

Abstract

Amino-terminal fragments from proteolytically cleaved gasdermins (GSDMs) form plasma membrane pores that enable the secretion of interleukin-1β (IL-1β) and IL-18. Excessive GSDM-mediated pore formation can compromise the integrity of the plasma membrane thereby causing the lytic inflammatory cell death, pyroptosis. We found that GSDMD and GSDME were the only GSDMs that were readily expressed in bone microenvironment. Therefore, we tested the hypothesis that GSDMD and GSDME are implicated in fracture healing owing to their role in the obligatory inflammatory response following injury. We found that bone callus volume and biomechanical properties of injured bones were significantly reduced in mice lacking either GSDM compared with wild-type (WT) mice, indicating that fracture healing was compromised in mutant mice. However, compound loss of GSDMD and GSDME did not exacerbate the outcomes, suggesting shared actions of both GSDMs in fracture healing. Mechanistically, bone injury induced IL-1β and IL-18 secretion *in vivo*, a response that was mimicked *in vitro* by bone debris and ATP, which function as inflammatory danger signals. Importantly, the secretion of these cytokines was attenuated in conditions of GSDMD deficiency. Finally, deletion of IL-1 receptor reproduced the phenotype of *Gsdmd* or *Gsdme* deficient mice, implying that inflammatory responses induced by the GSDM-IL-1 axis promote bone healing after fracture.

Introduction

Bone fractures are one of the most frequent injuries of the musculoskeletal system. Despite advances in therapeutic interventions, delayed healing, compromised quality of the newly regenerated bone, or nonunions remain frequent outcomes of these injuries (1, 2). These outcomes are complicated by the advanced age of the patients, infection, or sterile inflammation-prone comorbidities such as rheumatoid arthritis or diabetes mellitus (1-3). Although the recovery speed from fracture is greater in small animals such as rodents than in large counterparts and humans, the underlying repair mechanisms are shared across species (3). Thus, mouse models, which are amenable to genetic manipulation, provide opportunities for shedding light onto the mechanisms of fracture healing.

Bone fracture triggers an immediate inflammatory response during which neutrophils and macrophages are mobilized to the injury site to remove necrotic cells and debris while releasing factors that initiate neovascularization and promote tissue repair by recruiting mesenchymal progenitor cells from various sites such as the periosteum and bone marrow (3-5). The repair phase is followed by remodeling events where the balanced activity of osteoblasts and osteoclasts culminates in the restoration of the original bone structure and bone marrow cavity (4, 6, 7). Ultimately, inflammation subsides stemming from the suppressive actions of immune cells such as regulatory T cells, anti-inflammatory macrophages, and mesenchymal stem cells (8-10). Although inflammation declines over time, interfering with its onset immediately after injury can be detrimental as mice lacking interleukin-6 (IL-6), tumor necrosis factor-α (TNF-α), or macrophages exhibit defective healing (11-17). Thus, a fine-tuned level of inflammation is critical for adequate fracture healing.

IL-1β is another inflammatory cytokine that impacts fracture healing (18, 19). Unlike the aforementioned cytokines, IL-1β and IL-18 lack the signal peptide for secretion through the conventional endoplasmic reticulum and Golgi route. Expressed as pro-IL-1β and pro-IL-18,

these polypeptides are proteolytically activated by enzymes such as caspase-1, a component of the intracellular macromolecular complexes called inflammasomes (20, 21). Caspase-1 also cleaves GSDMD, generating GSDMD amino-terminal fragments, which form plasma membrane pores through which IL-1β and IL-18 are secreted to the extracellular milieu (21, 22). Although live cells can secrete these cytokines, excessive GSDMD-dependent pore formation compromises the integrity of the plasma membrane, causing a lytic form of cell death known as pyroptosis (22, 23). Pyroptotic cells release not only IL-1β and IL-18 but also other inflammatory molecules including eicosanoids, nucleotides, and alarmins (21, 22, 24). Thus, the actions of GSDMD in inflammatory settings can extend beyond the sole secretion of IL-1β and IL-18, and need to be tightly regulated to maintain homeostasis.

GSDMD is a member of the GSDM family proteins, which are encoded by *Gsdma1-3*, *Gsdmc1-4*, *Gsdmd*, and *Gsdme* also known as *Dnfa5* in the mouse genome (25). Mice lacking GSDMD are protected against multi-organ damage caused by gain-of-function mutations of nucleotide-binding oligomerization domain-like receptors family, pyrin domain containing 3 (NLRP3) or pyrin inflammasome (26, 27). GSDMD is also involved in the pathogenesis of complex diseases including experimental autoimmune encephalitis, radiation-induced tissue injury, ischemia/reperfusion injury, sepsis, renal fibrosis, and thrombosis (28-33). Other well studied GSDMs include GSDMA and GSDME (25, 34-36). GSDME is of particular interest to this study because recent evidence suggests that it harbors overlapping and non-overlapping actions with GSDMD, depending on cell contexts. Indeed, GSDME can mediate pyroptosis and release cytokines under both GSDMD sufficient and insufficient conditions (35, 37-40). Despite advances in GSDM studies, the role that these proteins play in fracture healing has not been studied. Since drugs for the treatment of GSDM-dependent inflammatory disorders and cancers are under development, it is imperative to understand their functions in the musculoskeletal system. Here, we found that loss of GSDMD or GSDME in mice impeded fracture healing through

mechanisms involving IL-1 signaling. This discovery has translational implications as drugs that inhibit GSDM functions may contribute to unsatisfactory fracture healing outcomes.

Materials and methods

Mice

Gsdmd knockout mice were kindly provided by Dr. V. M. Dixit (Genentech, South San Francisco, CA). All mice were on the C57BL6J background, and genotyping was performed by PCR. All procedures were approved by the Institutional Animal Care and Use Committee (IACUC) of Washington University School of Medicine in St. Louis.

Tibia fracture model

Open mid-shaft tibia fractures were created unilaterally in 12-week-old mice. Briefly, a 6-mm long incision was made in the skin on the anterior side alongside the tibia. A sterile 26-G needle was inserted into the tibia marrow cavity from the proximal end, temporarily withdrawn to allow transection of the tibia with a scalpel at mid-shaft, and then reinserted and secured. The incision was closed with 5-0 nylon sutures. Mice were sacrificed at different time-points as indicated below.

Histological analyses of fracture calluses

Fractured tibias were collected on day 7, 10, 14, 21, and 28 after fracture for histological analyses. Excess muscle and soft tissue were excised. Tibias were fixed in 10% neutral buffered formalin for 24 hours and decalcified for 10-14 days in 14% ethylenediaminetetraacetic acid solution (pH 7.2). Tissue was processed and embedded in paraffin, and sectioned longitudinally at a thickness of 5 µm. Alcian blue/hematoxylin/orange-g (ABH/OG) and tartrate-resistant acid phosphatase (TRAP) staining were performed to analyze the callus composition and osteoclast formation in the fracture region. Images were acquired using ZEISS microscopy (Carl Zeiss Industrial Metrology, MN). Cartilage area, bone area, mesenchyme area, and osteoclast

parameters were quantified on ABH/OG, TRAP-stained sections using NIH ImageJ software 1.52a (Wayne Rasband) and Bioquant (41).

Micro-computed tomography analysis

After careful dissection and removal of the intramedullary pins in fractured tibias, fracture calluses were examined using micro-computed tomography system (μCT 40 scanner, Scanco Medical AG, Zurich) scanner at 10 μm, 55 kVp, 145 μA, 300 ms integration time. Six hundred slices (6.3 mm) centered on the callus midpoint were used for micro-CT analyses. A contour was drawn around the margin of the entire callus and a lower threshold of 180 per mille was then applied to segment mineralized tissue (all bone inside the callus). A higher threshold of 340 per mille was applied to segment the original cortical bone inside the callus volume. Quantification for the volumes of the bone calluses was performed using the Scanco analysis software. 3D images were generated using a constant threshold of 180 per mille for the diaphyseal callus region of the fractured tibia.

Biomechanical torsion testing

Tibias were collected 28 days after fracture and moistened with PBS and stored at -20°C until they were thawed for biomechanical testing. Briefly, the ends of the samples were potted with methacrylate (MMA) bone cement (Lang Dental Manufacturing) in 1.2-cm-long cylinders (6-mm diameter). The fracture site was kept in the center of the two potted ends with roughly 4.2-mm of the bone exposed. After MMA solidification, potted bones were set up on a custom torsion machine. One end of the potted specimen was held in place while the opposing end was rotated at 1 degree per second until fracture. Torque values were plotted against the rotational deformation, and the maximum torque, torsional rigidity, and work to fracture were calculated.

Cell cultures

Murine primary bone marrow-derived macrophages (BMDMs) were obtained by culturing mouse bone marrow cells from femurs and tibias in culture media containing a 1:10 dilution of supernatant from the fibroblastic cell line CMG 14-12 as a source of macrophage colony-stimulating factor, a mitogenic factor for BMDMs, for 4-5 days in a 15-cm dish as previously described (29, 42). After expansion, BMDMs were plated at a density of 1 x 10^6 cells/well in 6-well plate for experiments.

Murine primary neutrophils were isolated by collecting bone marrow cells and subsequently over a discontinuous Percoll (Sigma) gradient. Briefly, all bone marrow cells from femurs and tibias were washed by DPBS and then resuspend in 2 mL DPBS. Cell suspension was gently layered on top of gradient (72% Percoll, 64% Percoll, 52% Percoll) and centrifuge at 1545 x g for 30 minutes at room temperature. After carefully discarding the top two cell layers, the third layer containing neutrophils was transferred to a clean 15 ml tube. Cells were washed and counted, then plated at a density of 3 x 10^6 cells/well in 6-well plate. Neutrophil purity was determined by flow cytometry showed in Figure S4.

For inflammasome studies, cells were primed with 100 ng/ml LPS (Sigma Aldrich, L4391) for 3 hours, then with 15 μM nigericin (Sigma Aldrich) for 1 hour, 5mM ATP for 1 hour, or 50 mg/ml bone particles for 2 hours.

Western blot

Cell extracts were prepared by lysing cells with RIPA buffer (50 mM Tris, 150 mM NaCl, 1 mM EDTA, 0.5% NaDOAc, 0.1% SDS, and 1.0% NP-40) plus complete protease inhibitor cocktail (Roche, CA). For tissue extracts, bone marrow (BM) and BM-free bones were lysed with RIPA buffer containing protease inhibitors. Protein concentrations were determined by the Bio-Rad Laboratories method, and equal amounts of proteins were subjected to SDS-PAGE gels (12%) as previously described (43). Proteins were transferred onto nitrocellulose membranes and incubated with antibodies against GSDMD (1:1000, ab219800, Abcam), GSDME (1:1000,

ab215191, Abcam), β-actin (1:5000, sc-47778, Santa Cruz Biotechnology, TX, USA) overnight at 4°C followed by incubation for 1 hour with secondary goat anti–mouse IRDye 800 (Thermo Fisher Scientific, MA) or goat anti–rabbit Alexa Fluor 680 (Thermo Fisher Scientific, MA), respectively. The results were visualized using the Odyssey infrared imaging system (LI-COR Biosciences, Lincoln, Nebraska, USA).

LDH assay

Cell death was assessed by the release of LDH in conditioned medium using LDH Cytotoxicity Detection Kit (TaKaRa, CA).

IL-1β and IL-18 ELISA

IL-1β, IL18 levels in conditioned media were measured by ELISA (eBiosciences, NY).

ATP assay

ATP levels in conditioned media were measured by RealTime-Glo Extracellular ATP Assay kit (Promega, WI).

Flow Cytometry

Bone marrow cells were flushed from tibias with PBS. Single cell suspensions were labeled with antibodies for 30 minutes at 4℃. Flow cytometry analysis was performed on FACS Canto II. Cell cytometric data was analyzed using FlowJo10.7.1. Full gating strategy was shown in Figures S4 and S5.

RNA isolation and RT-qPCR

RNA was extracted from bone or bone marrow cells using RNeasy Plus Mini Kit (Qiagen). Four millimeters of fracture calluses free of bone marrow were homogenized for mRNA extraction.

cDNA were prepared using High-Capacity cDNA Reverse Transcription Kits (Applied Biosystems). Gene expression was analyzed by qPCR using SYBR Green (Applied Biosystems) according to the manufacture.

Statistical analysis

Statistical analysis was performed using the Student's t test, one-way ANOVA with Tukey's multiple comparisons test as well as two-way ANOVA with Tukey's multiple comparisons test in GraphPad Prism 8.0 Software.

Results

GSDMD and GSDME were expressed in bone microenvironment

The crucial role that gasdermins (GSDMs) play in inflammation, a response that can be induced by injury, prompted us to analyze their expression in unfractured and fractured mouse tibias. *Gsdmd* and *Gsdme* were the only GSDM family members that were readily detected in bone marrow (BM) and BM-free tibias from wild-type (WT) mice (Fig. 1a-d, S1a and b; S2a and b). Expression levels of Gsdmd in BM and BM-free tibias (Fig. 1a-c; S2a) were consistently higher in fractured compared with unfractured bones. The injury did not affect *Gsdme* mRNA levels (Fig. 1a) but it increased Gsdme protein levels in BM-free tibias (Fig. S2b). Both GSDMs appeared constitutively cleaved in BM (Fig. 1c,d) but not BM-free tibias (Fig. S2a and b). Since Gsdmd was predominantly expressed in bones, we determined the impact of its loss on the expression of its family members. *Gsdmd* deficiency increased baseline *Gsdme* mRNA levels in BM-free tibias but not BM, a response that was unaffected by the injury and did not impact Gsdme protein levels (Fig. 1a-d; S2a, b). The expression of the other family members was unaltered by *Gsdmd* deficiency or the injury, with exception of *Gsdmc*, which was reduced in fractured BM-free tibias (Fig. S1a, b). Thus, GSDMD and GSDME are present in the bone microenvironment in homeostatic and injury states.

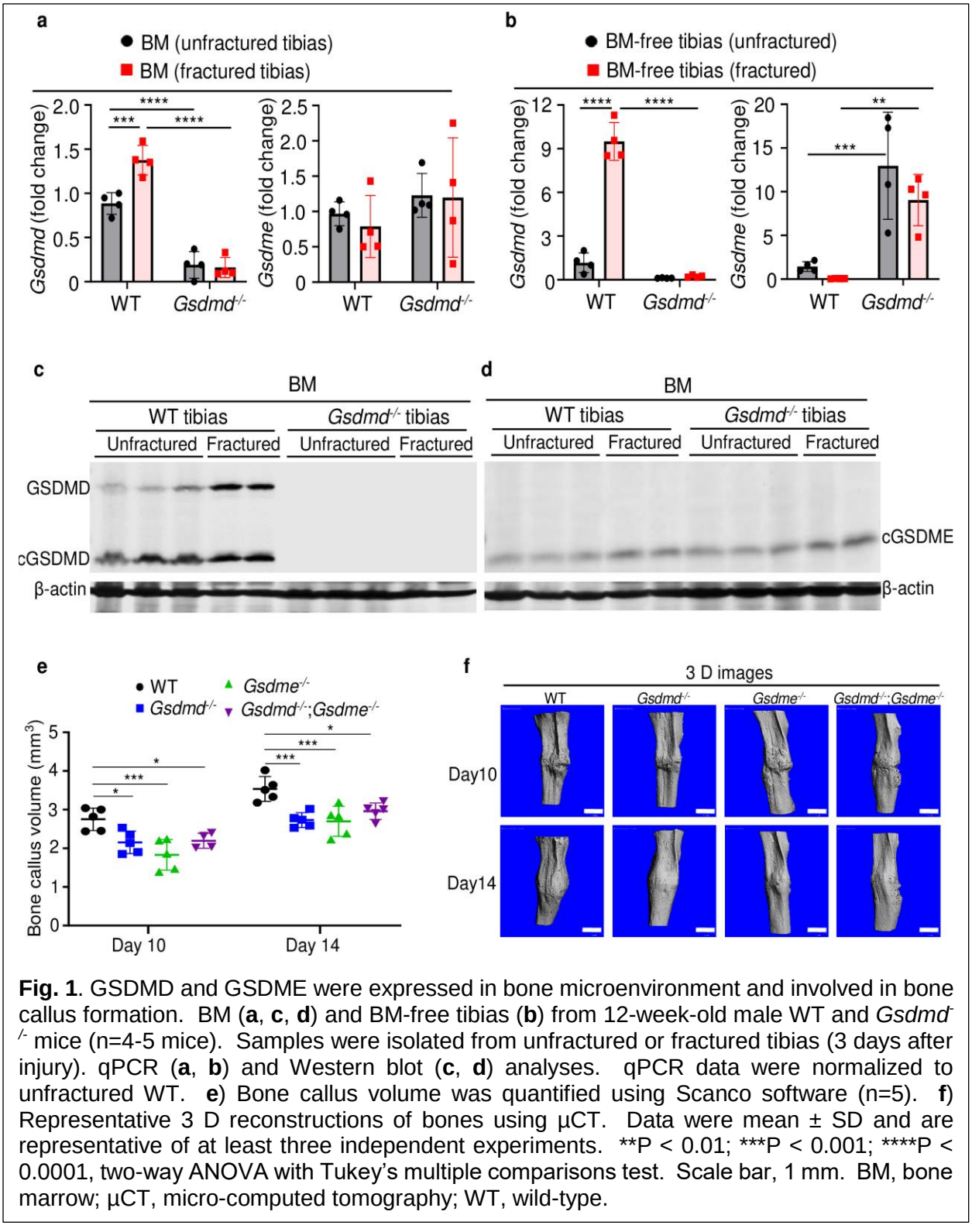

Fig. 1. GSDMD and GSDME were expressed in bone microenvironment and involved in bone callus formation. BM (**a**, **c**, **d**) and BM-free tibias (**b**) from 12-week-old male WT and *Gsdmd*$^{-/-}$ mice (n=4-5 mice). Samples were isolated from unfractured or fractured tibias (3 days after injury). qPCR (**a**, **b**) and Western blot (**c**, **d**) analyses. qPCR data were normalized to unfractured WT. **e**) Bone callus volume was quantified using Scanco software (n=5). **f**) Representative 3 D reconstructions of bones using µCT. Data were mean ± SD and are representative of at least three independent experiments. **P < 0.01; ***P < 0.001; ****P < 0.0001, two-way ANOVA with Tukey's multiple comparisons test. Scale bar, 1 mm. BM, bone marrow; µCT, micro-computed tomography; WT, wild-type.

Lack of GSDMD or GSDME delayed fracture healing

When stabilized with an intramedullary inserted pin, fractured murine long bones heal through mechanisms that involve the formation of callus structures (44). To determine the role of GSDMD and GSDME in fracture healing, we assessed callus formation in *Gsdmd*$^{-/-}$, *Gsdme*$^{-/-}$, and *Gsdmd*$^{-/-}$;*Gsdme*$^{-/-}$ mice. The volume of bone callus was higher on day 14 compared with day 10 post-injury in WT mice (Fig. 1e). It increased indistinguishably in *Gsdmd*$^{-/-}$ and *Gsdme*$^{-/-}$ mice on day 14 compared to day 10, but was significantly lower in mutants compared with WT mice (Fig. 1e, f). Notably, callus volume was comparable between single and compound mutants (Fig. 1e, f), suggesting that both GSDMs share the same signaling pathway in fracture healing. Collectively, these findings indicate that GSDMD and GSDME play an important role in bone repair following fracture injury.

To gain insights onto the mechanisms of fracture healing, we focused on GSDMD as its expression and proteolytic maturation were consistently induced by fracture. Time-course studies revealed that while the callus bone volume increased linearly until day 14 post-fracture and plateaued by day 21 in WT mice (Fig. 2a, b), it continued to expand in *Gsdmd*$^{-/-}$ mice until day 21 (Fig. 2a, b). The callus volume declined in both mouse strains by day 28 but it was larger in mutants compared with WT controls (Fig. 2a). Histological analysis indicated that the areas of the newly formed mesenchyme, cartilage, and bone were smaller in *Gsdmd*$^{-/-}$ compared with WT mice on day 7 (Fig. 2c-f). This outcome was also observed on day 10, except for the mesenchyme tissue area, which was larger in *Gsdmd*$^{-/-}$ compared with WT. While cartilage remnants were negligible in WT callus on day 14, they remained abundant in *Gsdmd*$^{-/-}$ counterparts (Fig. 2f). Additional histological assessments revealed that the number osteoclasts, which are involved in the remodeling of the newly formed bone, declined after day 14 not only in WT bones as expected, but also in mutants (Fig. 2g-i). At any time-point, there were more osteoclasts in injured *Gsdmd*$^{-/-}$ bones compared to WT counterparts. Taken together, these results suggest that the healing process is perturbed in mutant mice.

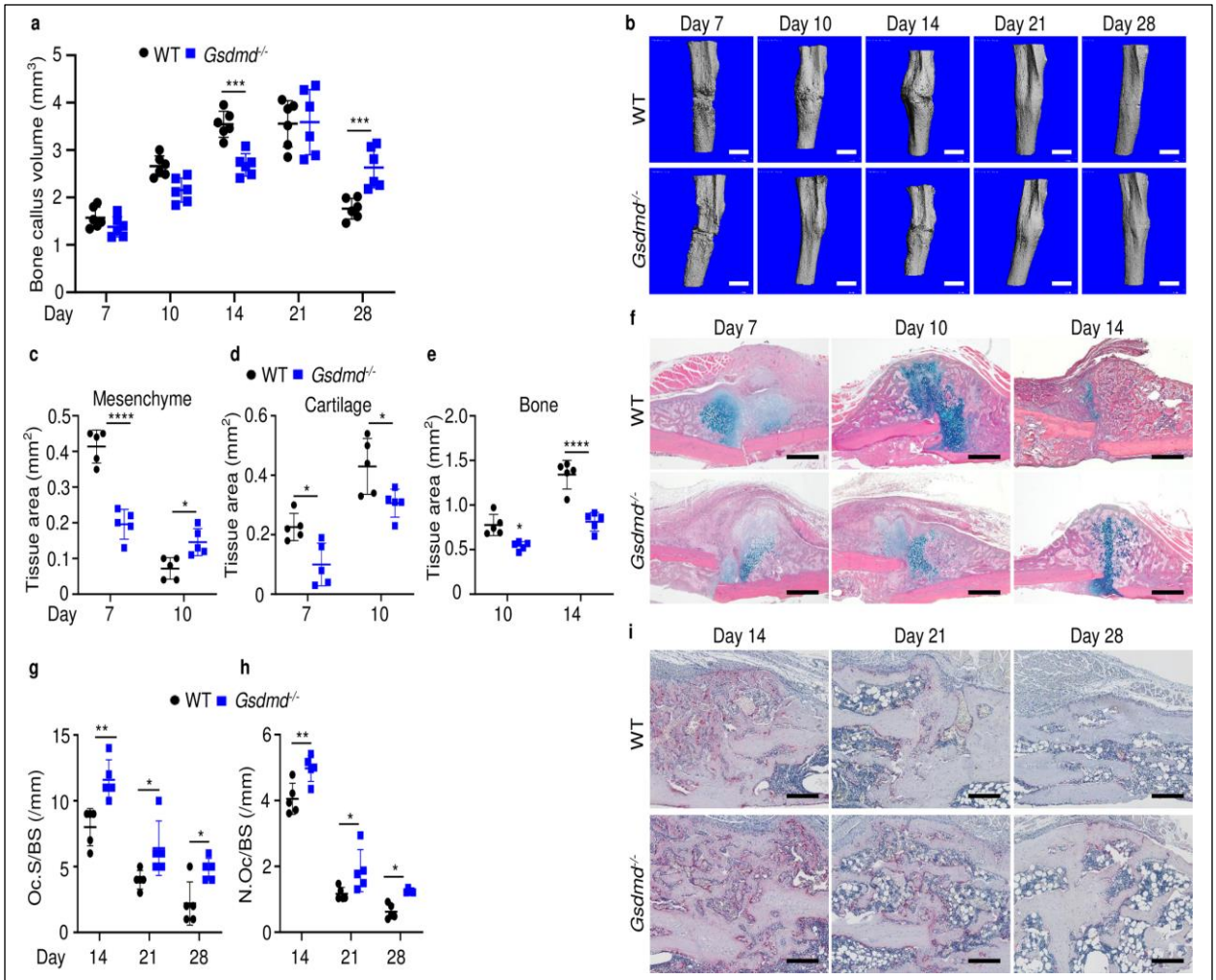

Fig. 2. Loss of GSDMD delayed fracture healing. Tibias of 12-week-old male and female WT or *Gsdmd*$^{-/-}$ mice were subjected to fracture and analyzed at the indicated times. **a**) Bone callus volume was quantified using Scanco software (n=6). **b**) Representative 3 D reconstructions of bones using µCT. **c**, **d**, **e**) Quantification of tissue area by imageJ software (n=5). **f**) Representative ABH staining. Quantification of Oc.S/BS (**g**) and N.Oc/BS (**h**) using Bioquant software (n=5). **i**) Representative images of TRAP staining. Data were mean ± SD. *P < 0.05; ***P < 0.001; ****P < 0.0001, two-way ANOVA with Tukey's multiple comparisons test. Scale bar, 1 mm (**b**), 500 µm(**f**) ,or 200 µm(**i**) µm. µCT, micro-computed tomography; WT, wild-type.

To determine the impact of GSDMD deficiency on the functional result of bone regeneration, unfractured and 28-day post fracture bones were subjected to biomechanical testing. Injured WT tibias exhibited decreased strength an stiffness compared with unfractured counterparts (Fig. 3a-c), indicating that the healing response has not fully recovered bone function at this time-point. Biomechanical properties of unfractured *Gsdmd*$^{-/-}$ tibias were slightly higher though not statistically significant in *Gsdmd*$^{-/-}$ compared with WT unfractured bones (Fig. 3a-c), findings that were consistent with the higher bone mass phenotype of *Gsdmd*$^{-/-}$ mice relative to their littermates (29). Notably, fractured bones from *Gsdmd*$^{-/-}$ mice exhibited lower biomechanical parameters compared with WT controls. Thus, the functional competence of the repaired bone structure is compromised in GSDMD deficient mice.

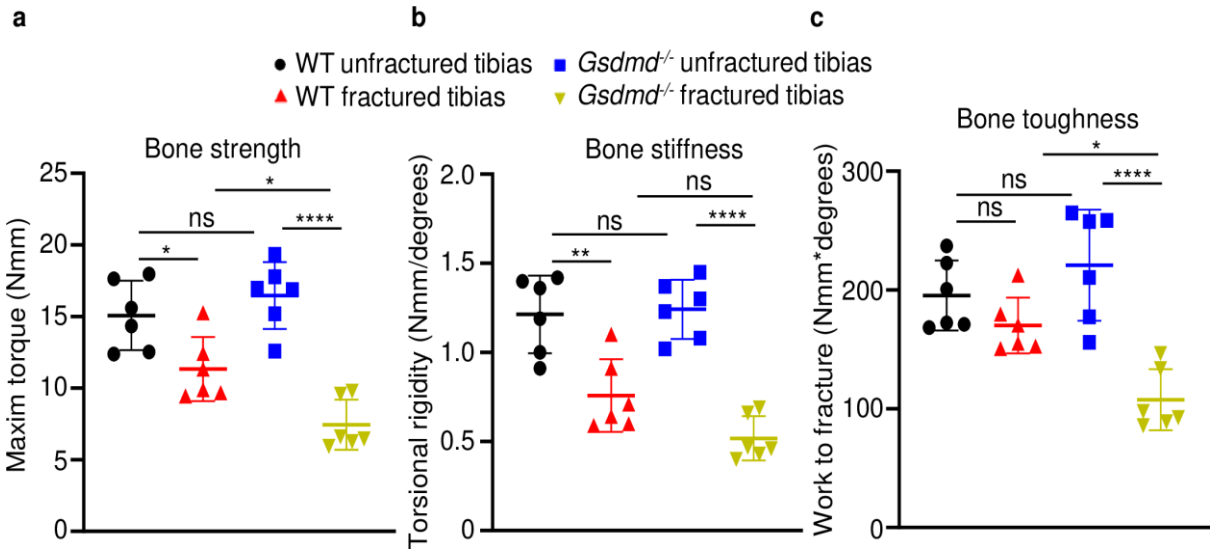

Fig. 3. Loss of GSDMD compromised bone biomechanical properties after fracture. Unfractured or fractured tibias (28 days after injury) from 12-week-old male WT or *Gsdmd*$^{-/-}$ mice were subjected to a torsion test (n=6). **a**) Bone strength. **b**) Bone stiffness. **c**) Bone toughness. Data were mean ± SD. *P < 0.05; **P < 0.01; ****P < 0.0001, One-way ANOVA with Tukey's multiple comparisons test. ns, non significant WT, wild-type.

Expression and secretion of IL-1β and IL-18 were attenuated in the absence of GSDMD

Inflammation characterized by elevated levels of cytokines including those of the IL-1 family underlines the early phase of wound healing (3). Since IL-1β and IL-18 are secreted through GSDMD-assembled plasma membrane pores (21-23), we analyzed the levels of these inflammatory cytokines in the bone marrow supernatants from unfractured and fractured bones (1 day after injury). Baseline secretion levels of IL-1β or IL-18 were comparable between WT and *Gsdmd* mutants (Fig. 4a, b). Fracture increased IL-1β and IL-18 levels in bone marrow supernatants in both groups, but they were significantly attenuated in mutant samples compared with WT controls (Fig. 4a, b). Thus, fracture-induced IL-1β and IL-18 levels in bone marrow are attenuated upon loss of GSDMD.

To understand transcriptional regulation of IL-1β and IL-18 in this fracture model, we determined mRNA levels of these cytokines in the BM and BM-free bone compartments. Baseline levels of *Il1b* and *Il18* mRNA were undistinguishable between WT and *Gsdmd*$^{-/-}$ samples in both compartments (Fig. 4c, d). Following fracture, the expression of *Il1b* and *Il18* mRNA was induced in WT but not *Gsdmd*$^{-/-}$ mice (Fig. 4c,d), suggesting a feedback mechanism whereby these cytokines secreted though GSDMD pores amplified their own expression. Since NLRP3 and absent in melanoma 2 (AIM2) inflammasomes, which sense plasma stimuli such as membrane perturbations and DNA, respectively, are implicated in the maturation of IL-1β, IL-18, and GSDMD (26, 29, 45), we also analyzed the expression of these sensors. Levels of *Nlrp3* and *Aim2* to some extent (Fig. 4c, d) as well as those of *Asc* and caspase-1 (Fig. S3a, b) were comparable between WT and *Gsdmd*$^{-/-}$ samples in homeostatic conditions. Fracture increased the expression of *Nlrp3* and *Aim2* in WT and mutants only in BM-free bone samples (Fig. 4c, d) whereas it induced caspase-1 expression WT cells both compartments. Never was the expression of *Nlrc4* and caspase-11 mRNA modulated by the fracture injury nor loss of GSDMD (Fig. S3a, b). Thus, the expression of *Il1b* or *Il18* and certain inflammasome components (e.g., *Nlrp3*, *Aim2*, *Asc*, and caspase-1) is transcriptionally regulated in the fracture injury model.

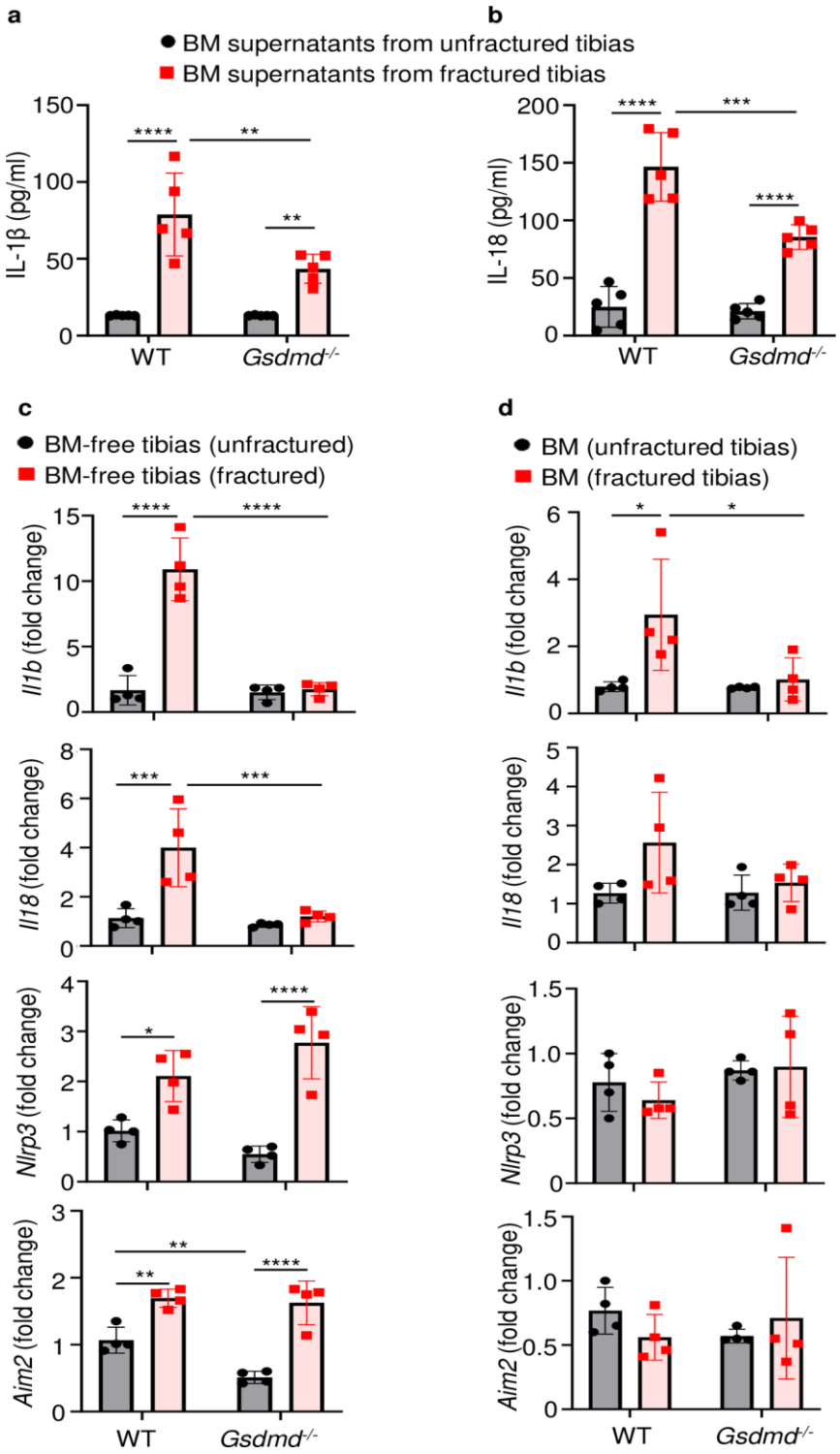

Fig. 4. Loss of GSDMD attenuated the expression and secretion of IL-1β and IL-18 induced by fracture. BM supernatants (**a**, **b**) and BM-free bones (**c**) were from 12-week-old male WT or *Gsdmd*$^{-/-}$ mice (n=4-5). Samples were isolated from unfractured or fractured tibias (1 day after injury). ELISA (**a**, **b**) and qPCR (**c**, **d**) analyses. qPCR data were normalized to unfractured WT. Data were mean ± SD. *P < 0.05; **P < 0.01; ***P < 0.001; ****P < 0.0001, two-way ANOVA with Tukey's multiple comparisons test. BM, bone marrow; WT, wild-type.

Lack of GSDMD attenuated the secretion of IL-1β and IL-18 induced by danger signals

The high levels IL-1β and IL-18 in bone marrow of fractured bones provided a strong rationale for assessing the presence of neutrophils, monocytes, and macrophages, which harbor high levels of inflammasomes and rapidly accumulate during the first hours after injury (25, 26, 29). Flow cytometry analysis revealed that the abundance of these cells in bone marrow of uninjured bones was unaffected by loss of GSDMD (Fig. 5a-c; S5). Fracture increased the percentage of neutrophils and monocytes but not macrophages (Fig. 5a-c). GSDMD deficiency was associated with a slight decrease and increase in the percentage of neutrophils and monocytes, respectively (Fig. 5a-c). Thus, neutrophil and monocyte but not macrophage populations are expanded in fractured bones. GSDMD deficiency appears to slightly attenuate and increase the percentage of neutrophils and monocytes, respectively.

Inflammasome assembly signals include those generated by ATP, which is released by dead cells (46, 47). Therefore, we measured the levels of this danger signal in bone marrow. ATP levels were comparable between WT and *Gsdmd*$^{-/-}$ samples at baseline but were induced by 4-fold after fracture in both groups (Fig. 5d). Next, we studied cytokine release by WT and *Gsdmd*$^{-/-}$ cells not only in response to ATP but also bone particles, which are undoubtedly released following bone fracture. Bone particles were as potent as the NLRP3 inflammasome activators, nigericin and ATP, in inducing GSDMD cleavage by LPS-primed macrophages (Fig. 5e). Accordingly, these danger signals induced IL-1β release (Fig. 5f) and pyroptosis as assessed by the release of lactate dehydrogenase (LDH; Fig. S6a), responses that were attenuated in GSDMD-deficient macrophages. Both nigericin and ATP robustly stimulated GSDMD cleavage and IL-1β release by LPS-primed neutrophils through mechanisms that partially involved GSDMD, but only nigericin caused neutrophil pyroptosis (Fig. S6b). Bone particles had no effect on GSDMD maturation and IL-1β and LDH release by neutrophils (Fig. 5g, h and Fig. S6b). Thus, fracture injury creates a microenvironment that induces cytokine secretion through mechanisms involving GSDMD.

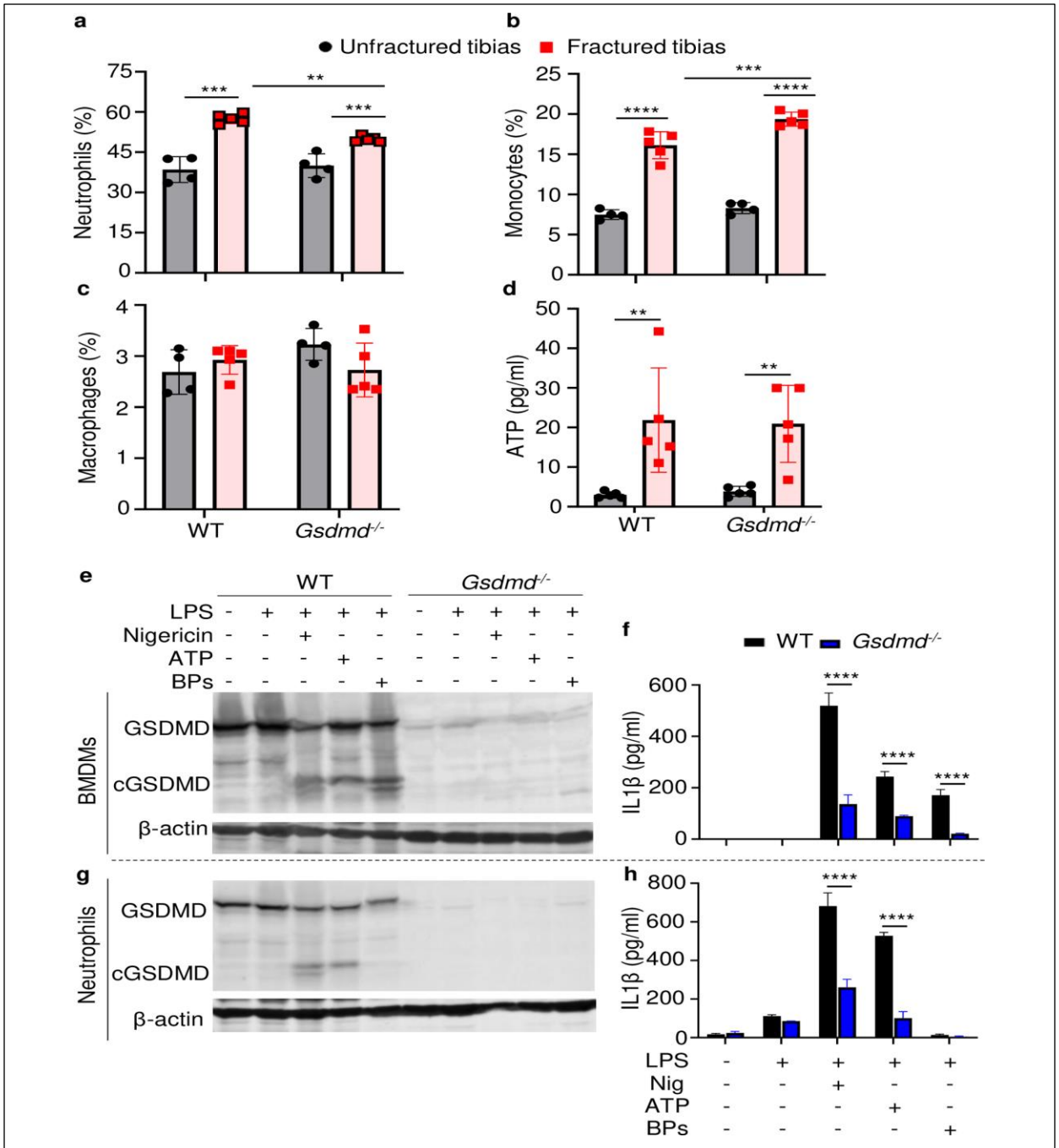

Fig. 5. Loss of GSDMD attenuated the secretion of IL-1β and IL-18 induced by danger signals. Cells were isolated from the tibias from 12-week-old female WT or *Gsdmd*$^{-/-}$ mice. **a**, **b**, **c**) Cell counts (n=4-5). BM was harvested from unfractured or fractured tibias (2 days after fracture). **d**) ATP levels. BM supernatants were harvested from unfractured or fractured tibias (24 hours after fracture). Immunoblotting analysis of GSDMD cleavage (**e**, **g**) or IL-1β ELISA run in triplicates (**f**, **h**). BMDMs were expanded *in vitro* whereas neutrophils were immediately after purification. Cells were primed with 100 ng/ml LPS for 3 hours, then with 15 μM nigericin for 1 hour, 5 mM ATP for 1 hour, or 50 mg/ml bone particles for 2 hours. Data are mean ± SD and were representative of at least three independent experiments. *P < 0.05; **P < 0.01; ***P < 0.001; ****P < 0.0001, two-way ANOVA with Tukey's multiple comparisons test. BPs, bone particles; cGSDMD, cleaved GSDMD; WT, wild-type.

Loss of IL-1 signaling delayed fracture healing

The inability of *Gsdmd*$^{-/-}$ mice to mount efficient healing responses correlated with low levels of IL-1β and IL-18 in bone marrow, suggesting that inadequate secretion of these cytokines may account for the delayed fracture repair. While the actions of IL-18 in bone are not well defined, overwhelming evidence positions IL-1β as a key regulator of skeletal pathophysiology (48, 49). Therefore, we used IL-1 receptor knockout (*Il1r*$^{-/-}$) mice to test the hypothesis that IL-1 signaling was required for bone healing following fracture. Bone callus volume was larger on day 14 compared with day 10 in WT and *Il1r*$^{-/-}$ tibias, but it was smaller at both time-points in mutants compared to WT controls (Fig. 6a, b). Histological analysis confirmed that the mesenchyme, cartilage, and bone areas were all smaller in *Il1r*$^{-/-}$ compared with WT mice (Fig. 6c-f). Like in *Gsdmd*$^{-/-}$ tissues, cartilage remnants were prominent within the callus of *Il1r*$^{-/-}$ specimens at day 14 (Fig. 6f), and the number and surface of osteoclasts were significantly higher at all times in mutant compared to WT mice at day 7, while cartilage and bone areas remained smaller in mutants at day 10 (Fig. 6g-i). Thus, *Il1r*$^{-/-}$ mice phenocopy the delayed healing patterns of *Gsdmd*$^{-/-}$ mice, suggesting that functional GSDMD-IL-1 axis is important for adequate bone healing after fracture.

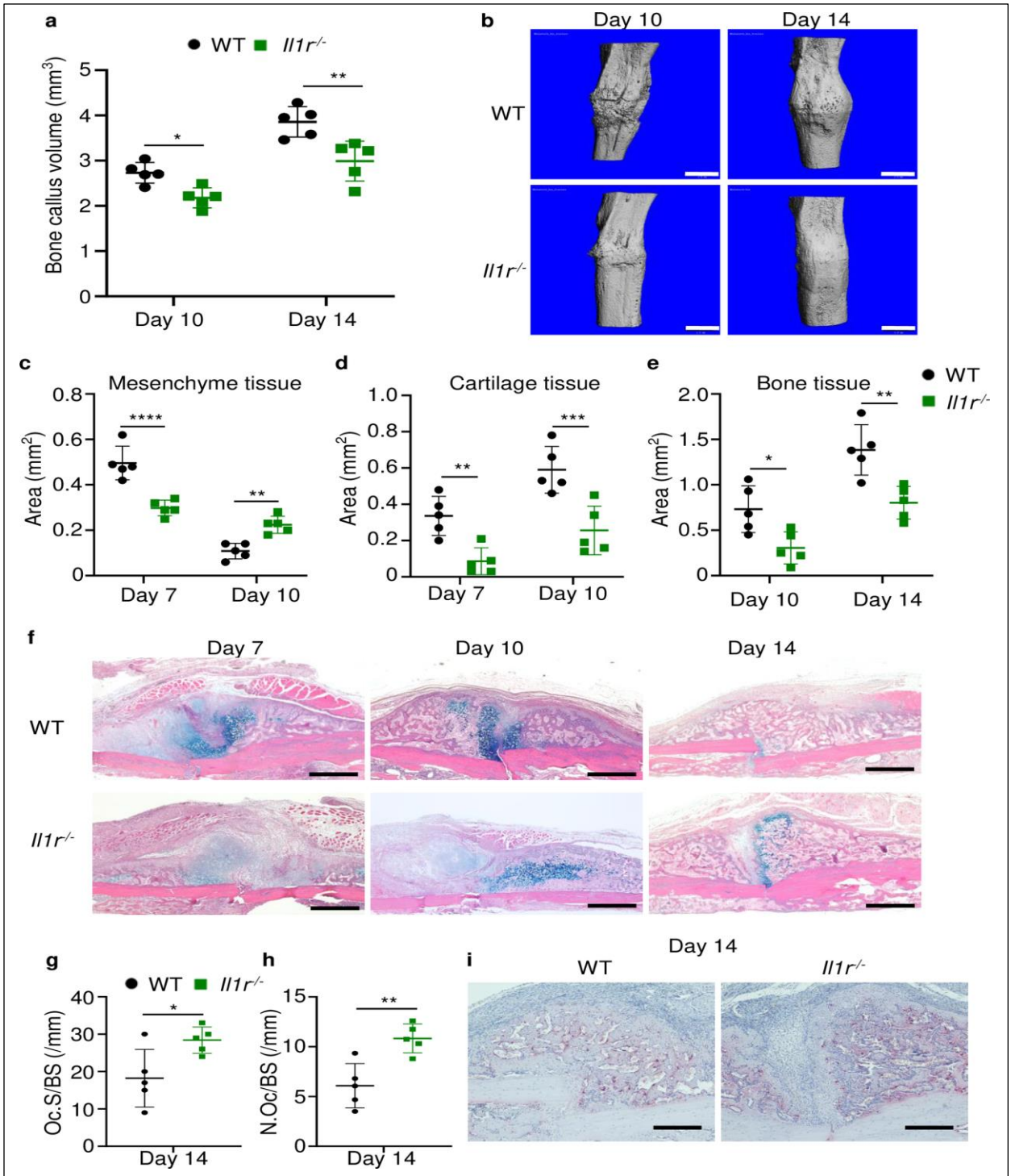

Fig. 6. Loss of IL-1 receptor delayed fracture healing. Tibias of 12-week-old male WT or *Il1r*$^{-/-}$ mice were subjected to fracture and analyzed at the indicated times. **a**) Bone callus volume was quantified using Scanco software (n=5). **b**) Representative 3 D reconstructions of bones using µCT. **c**, **d**, **e**) Quantification of tissue area by imageJ software (n=5). **f**) Representative ABH staining. Quantification of Oc.S/BS (**g**) and Oc.S/BS (**h**) using Bioquant software (n=5). **i**) Representative images of TRAP staining. Data were mean ± SD. *P < 0.05; ***P < 0.001; ****P < 0.0001, two-way ANOVA with Tukey's multiple comparisons test (**a**, **c**, **d**, **e**) or unpaired t-test (**g**, **h**). Scale bar, 1 mm (**b**), 500 µm (**f**) or 200 µm (**i**). *Il1r*, IL-1 receptor; WT, wild-type.

Discussion

GSDMs are implicated in a variety of inflammatory diseases but their role in bone regeneration after fracture is largely unknown. We found that fracture healing was comparably delayed in mice lacking GSDMD or GSDME; yet concomitant loss of GSDMD and GSDME did not worsen the phenotype. This outcome was unexpected because these GSDMs are activated via distinct mechanisms as GSDMD is cleaved by caspase-11 (mouse ortholog of human caspase-4 and -5), neutrophil elastase and cathepsin G, or caspase-8 whereas GSDME is processed by caspase-3 and granzyme B (34, 39). The phenotype of double knockout mice suggested complex, and possibly convergent actions of these GSDMs in fracture healing. Indeed, the phenotype of either single mutant strain implied non-redundant functions of both GSDMs whereas the outcomes of compound mutants suggested that they shared downstream effector molecules. The latter view was supported by the ability of either GSDM to mediate pyroptosis and IL-1β and IL-18 release in cell a context-dependent manner (35, 37-40). Furthermore, functional complementation of GSDMD by GSDME has also been reported (35). Thus, although additional studies are needed for further insights onto the mechanism of differential actions of GSDMD and GSDME in bone recovery after injury, our findings reinforce the crucial role that inflammation plays during the bone fracture healing process.

In addition to IL-1β and IL-18, inflammatory mediators such as ATP, alarmins (e.g., IL-1α, S100A8/9, high mobility group box 1, and eicosanoids (e.g., PGE_2) are expected to be uncontrollably released during pyroptosis (24, 50). Since these inflammatory and danger signals work in concert to inflict maximal tissue damage, we anticipated a milder delay in fracture healing in mice lacking IL-1 receptor compared with GSDM deficient mice. Contrary to our expectation, callus volumes and the recovery time were comparable among all mutant mouse strains. These observations suggested that IL-1 signaling downstream of GSDMs played a non-redundant role in fracture healing. This view was consistent with the reported essential role of IL-1α and IL-1β in bone repair and aligned with the high expression of these cytokines by immune cells, which are

known to massively infiltrate the fracture site (3). Thus, although IL-1 signaling has been extensively studied in various injury contexts, the novelty of this work is its demonstration of the role of GSDM-IL-1 axis in fracture repair.

IL-1 signaling induces the expression of cytokines, chemokines, and growth factors that govern bone remodeling, a process that is initiated by the osteoclasts (51). Consistent with the critical actions of GSDM-IL-1 cascades in bone repair and the osteoclastogenic actions of IL-1β, loss of GSDMD in mice resulted in increased bone mass at baseline as the result of decreased osteoclast differentiation (29). Here, we found that lack of GSDMD was associated with increased number of osteoclasts and their precursors, the monocytes. We surmised that this result was simply a reflection of retarded osteoclastogenesis in mutant mice as the consequence of delayed responses such as neovascularization and development of bone marrow cavity. This view is based by the fact that bone marrow is the site of hematopoiesis in adult animals and vascularization is important for the traffic of osteoclast progenitors. As a result, disruption in either hematopoiesis or vascularization should undoubtedly impact osteoclastogenesis (52).

Fracture injury increased the levels of Nlrp3 and its activator ATP in bone marrow, suggesting that the inflammasome assembled by this sensor may be responsible for the activation of GSDMs, particularly, GSDMD. However, more studies are needed to firm up this conclusion since Aim2 was also expressed in bone marrow. Other limitations of this study included i) the lack of data comparing biomechanical properties of fractured bones from all the mutant mouse strains used, ii) the unknown function of IL-18 pathway in fracture healing, and iii) the knowledge gap on differential expression of GSDMD and GSDME by the various cell types that are activated in response to fracture. Despite these shortcomings, this study has revealed the crucial role that GSDMD and GSDME play in fracture healing. It also suggests that drugs that inhibit the functions of these GSDMs may have adverse effects on this healing process.

Acknowledgements

This work was supported by NIH/NIAMS AR076758 and AI161022 grants to GM. JS was supported by NIH grants AR075860, AR077616, and AR077226; YA-A by NIH grants AR049192, AR074992, AR072623, and by grant #85160 from the Shriners Hospital for Children; MJS., by NIH grants AR074992.

Conflict of interests

Dr. Gabriel Mbalaviele is consultant for Aclaris Therapeutics, Inc. All other authors declare no conflict of interest.

Contributions

Study conception and design: KS, GM

Acquisition of data and methodology: KS, CW, MB, LY, TY, YA, HH, DH, YA-A, MS, JS

Analysis and interpretation of data: KS, CW, MDB, LY, TY, YA, YA-A, MJS, JS

Editing: KS, MDB, LY, MJS

Writing: KS, GM

References

1. Clement ND, Beauchamp NJ, Duckworth AD, McQueen MM, Court-Brown CM. The outcome of tibial diaphyseal fractures in the elderly. Bone Joint J. 2013;95-B(9):1255-62. Epub 2013/09/03. doi: 10.1302/0301-620X.95B9.31112. PubMed PMID: 23997142.
2. Muire PJ, Mangum LH, Wenke JC. Time Course of Immune Response and Immunomodulation During Normal and Delayed Healing of Musculoskeletal Wounds. Front Immunol. 2020;11:1056. Epub 2020/06/26. doi: 10.3389/fimmu.2020.01056. PubMed PMID: 32582170; PMCID: PMC7287024.
3. Claes L, Recknagel S, Ignatius A. Fracture healing under healthy and inflammatory conditions. Nat Rev Rheumatol. 2012;8(3):133-43. Epub 2012/02/02. doi: 10.1038/nrrheum.2012.1. PubMed PMID: 22293759.
4. Colnot C, Huang S, Helms J. Analyzing the cellular contribution of bone marrow to fracture healing using bone marrow transplantation in mice. Biochem Biophys Res Commun. 2006;350(3):557-61. Epub 2006/10/07. doi: 10.1016/j.bbrc.2006.09.079. PubMed PMID: 17022937.
5. Glass GE, Chan JK, Freidin A, Feldmann M, Horwood NJ, Nanchahal J. TNF-alpha promotes fracture repair by augmenting the recruitment and differentiation of muscle-derived stromal cells. Proc Natl Acad Sci U S A. 2011;108(4):1585-90. Epub 2011/01/07. doi: 10.1073/pnas.1018501108. PubMed PMID: 21209334; PMCID: PMC3029750.
6. Hardy R, Cooper MS. Bone loss in inflammatory disorders. J Endocrinol. 2009;201(3):309-20. Epub 2009/05/16. doi: 10.1677/JOE-08-0568. PubMed PMID: 19443863.
7. Xing Z, Lu C, Hu D, Yu YY, Wang X, Colnot C, Nakamura M, Wu Y, Miclau T, Marcucio RS. Multiple roles for CCR2 during fracture healing. Dis Model Mech. 2010;3(7-8):451-8. Epub 2010/04/01. doi: 10.1242/dmm.003186. PubMed PMID: 20354109; PMCID: PMC2898536.
8. Al-Sebaei MO, Daukss DM, Belkina AC, Kakar S, Wigner NA, Cusher D, Graves D, Einhorn T, Morgan E, Gerstenfeld LC. Role of Fas and Treg cells in fracture healing as characterized in the fas-deficient (lpr) mouse model of lupus. J Bone Miner Res. 2014;29(6):1478-91. Epub 2014/03/29. doi: 10.1002/jbmr.2169. PubMed PMID: 24677136; PMCID: PMC4305200.
9. Nauta AJ, Fibbe WE. Immunomodulatory properties of mesenchymal stromal cells. Blood. 2007;110(10):3499-506. Epub 2007/08/01. doi: 10.1182/blood-2007-02-069716. PubMed PMID: 17664353.
10. Noel D, Djouad F, Bouffi C, Mrugala D, Jorgensen C. Multipotent mesenchymal stromal cells and immune tolerance. Leuk Lymphoma. 2007;48(7):1283-9. Epub 2007/07/07. doi: 10.1080/10428190701361869. PubMed PMID: 17613755.
11. Yang X, Ricciardi BF, Hernandez-Soria A, Shi Y, Pleshko Camacho N, Bostrom MP. Callus mineralization and maturation are delayed during fracture healing in interleukin-6 knockout mice. Bone. 2007;41(6):928-36. Epub 2007/10/09. doi: 10.1016/j.bone.2007.07.022. PubMed PMID: 17921078; PMCID: PMC2673922.
12. Wallace A, Cooney TE, Englund R, Lubahn JD. Effects of interleukin-6 ablation on fracture healing in mice. J Orthop Res. 2011;29(9):1437-42. Epub 2011/03/30. doi: 10.1002/jor.21367. PubMed PMID: 21445992.
13. Gerstenfeld LC, Cho TJ, Kon T, Aizawa T, Tsay A, Fitch J, Barnes GL, Graves DT, Einhorn TA. Impaired fracture healing in the absence of TNF-alpha signaling: the role of TNF-alpha in endochondral cartilage resorption. J Bone Miner Res. 2003;18(9):1584-92. Epub 2003/09/13. doi: 10.1359/jbmr.2003.18.9.1584. PubMed PMID: 12968667.
14. Baht GS, Silkstone D, Vi L, Nadesan P, Amani Y, Whetstone H, Wei Q, Alman BA. Erratum: Exposure to a youthful circulation rejuvenates bone repair through modulation of beta-catenin. Nat Commun. 2015;6:7761. Epub 2015/08/27. doi: 10.1038/ncomms8761. PubMed PMID: 26307670; PMCID: PMC4647860.

15. Raggatt LJ, Wullschleger ME, Alexander KA, Wu AC, Millard SM, Kaur S, Maugham ML, Gregory LS, Steck R, Pettit AR. Fracture healing via periosteal callus formation requires macrophages for both initiation and progression of early endochondral ossification. Am J Pathol. 2014;184(12):3192-204. Epub 2014/10/07. doi: 10.1016/j.ajpath.2014.08.017. PubMed PMID: 25285719.
16. Xing Z, Lu C, Hu D, Miclau T, 3rd, Marcucio RS. Rejuvenation of the inflammatory system stimulates fracture repair in aged mice. J Orthop Res. 2010;28(8):1000-6. Epub 2010/01/29. doi: 10.1002/jor.21087. PubMed PMID: 20108320; PMCID: PMC2892015.
17. Chang MK, Raggatt LJ, Alexander KA, Kuliwaba JS, Fazzalari NL, Schroder K, Maylin ER, Ripoll VM, Hume DA, Pettit AR. Osteal tissue macrophages are intercalated throughout human and mouse bone lining tissues and regulate osteoblast function in vitro and in vivo. J Immunol. 2008;181(2):1232-44. Epub 2008/07/09. doi: 10.4049/jimmunol.181.2.1232. PubMed PMID: 18606677.
18. Einhorn TA, Majeska RJ, Rush EB, Levine PM, Horowitz MC. The expression of cytokine activity by fracture callus. J Bone Miner Res. 1995;10(8):1272-81. Epub 1995/08/01. doi: 10.1002/jbmr.5650100818. PubMed PMID: 8585432.
19. Morisset S, Frisbie DD, Robbins PD, Nixon AJ, McIlwraith CW. IL-1ra/IGF-1 gene therapy modulates repair of microfractured chondral defects. Clin Orthop Relat Res. 2007;462:221-8. Epub 2007/05/31. doi: 10.1097/BLO.0b013e3180dca05f. PubMed PMID: 17534189.
20. Schroder K, Tschopp J. The inflammasomes. Cell. 2010;140(6):821-32. Epub 2010/03/23. doi: 10.1016/j.cell.2010.01.040. PubMed PMID: 20303873.
21. Broz P, Dixit VM. Inflammasomes: mechanism of assembly, regulation and signalling. Nat Rev Immunol. 2016;16(7):407-20. Epub 2016/06/14. doi: 10.1038/nri.2016.58. PubMed PMID: 27291964.
22. Shi J, Zhao Y, Wang K, Shi X, Wang Y, Huang H, Zhuang Y, Cai T, Wang F, Shao F. Cleavage of GSDMD by inflammatory caspases determines pyroptotic cell death. Nature. 2015;526(7575):660-5. Epub 2015/09/17. doi: 10.1038/nature15514. PubMed PMID: 26375003.
23. Evavold CL, Ruan J, Tan Y, Xia S, Wu H, Kagan JC. The Pore-Forming Protein Gasdermin D Regulates Interleukin-1 Secretion from Living Macrophages. Immunity. 2018;48(1):35-44 e6. Epub 2017/12/03. doi: 10.1016/j.immuni.2017.11.013. PubMed PMID: 29195811; PMCID: PMC5773350.
24. Rauch I, Deets KA, Ji DX, von Moltke J, Tenthorey JL, Lee AY, Philip NH, Ayres JS, Brodsky IE, Gronert K, Vance RE. NAIP-NLRC4 Inflammasomes Coordinate Intestinal Epithelial Cell Expulsion with Eicosanoid and IL-18 Release via Activation of Caspase-1 and -8. Immunity. 2017;46(4):649-59. Epub 2017/04/16. doi: 10.1016/j.immuni.2017.03.016. PubMed PMID: 28410991; PMCID: PMC5476318.
25. Liu X, Xia S, Zhang Z, Wu H, Lieberman J. Channelling inflammation: gasdermins in physiology and disease. Nat Rev Drug Discov. 2021;20(5):384-405. Epub 2021/03/12. doi: 10.1038/s41573-021-00154-z. PubMed PMID: 33692549; PMCID: PMC7944254.
26. Xiao J, Wang C, Yao JC, Alippe Y, Xu C, Kress D, Civitelli R, Abu-Amer Y, Kanneganti TD, Link DC, Mbalaviele G. Gasdermin D mediates the pathogenesis of neonatal-onset multisystem inflammatory disease in mice. PLoS Biol. 2018;16(11):e3000047. Epub 2018/11/06. doi: 10.1371/journal.pbio.3000047. PubMed PMID: 30388107; PMCID: PMC6235378 following competing interests: GM is a consultant for Aclaris Therapeutics, Inc., and holds stocks of this company. RC receives research support from Amgen, and holds stock of Amgen, Eli- Lilly, and Merck & Co.
27. Kanneganti A, Malireddi RKS, Saavedra PHV, Vande Walle L, Van Gorp H, Kambara H, Tillman H, Vogel P, Luo HR, Xavier RJ, Chi H, Lamkanfi M. GSDMD is critical for autoinflammatory pathology in a mouse model of Familial Mediterranean Fever. J Exp Med. 2018;215(6):1519-29. Epub 2018/05/26. doi: 10.1084/jem.20172060. PubMed PMID: 29793924; PMCID: PMC5987922.

28. Li S, Wu Y, Yang D, Wu C, Ma C, Liu X, Moynagh PN, Wang B, Hu G, Yang S. Gasdermin D in peripheral myeloid cells drives neuroinflammation in experimental autoimmune encephalomyelitis. J Exp Med. 2019;216(11):2562-81. Epub 2019/08/31. doi: 10.1084/jem.20190377. PubMed PMID: 31467036; PMCID: PMC6829591.
29. Xiao J, Wang C, Yao JC, Alippe Y, Yang T, Kress D, Sun K, Kostecki KL, Monahan JB, Veis DJ, Abu-Amer Y, Link DC, Mbalaviele G. Radiation causes tissue damage by dysregulating inflammasome-gasdermin D signaling in both host and transplanted cells. PLoS Biol. 2020;18(8):e3000807. Epub 2020/08/08. doi: 10.1371/journal.pbio.3000807. PubMed PMID: 32760056; PMCID: PMC7446913 following competing interests: GM is a consultant for Aclaris Therapeutics. KLK and JBM are employees of Aclaris Therapeutics.
30. Zhang D, Qian J, Zhang P, Li H, Shen H, Li X, Chen G. Gasdermin D serves as a key executioner of pyroptosis in experimental cerebral ischemia and reperfusion model both in vivo and in vitro. J Neurosci Res. 2019;97(6):645-60. Epub 2019/01/03. doi: 10.1002/jnr.24385. PubMed PMID: 30600840.
31. Silva CM, Wanderley CWS, Veras FP, Sonego F, Nascimento DC, Goncalves AV, Martins TV, Colon DF, Borges VF, Brauer VS, Damasceno LEA, Silva KP, Toller-Kawahisa JE, Batah SS, Souza ALJ, Monteiro VVS, Oliveira AER, Donate PB, Zoppi D, Borges MC, Almeida F, Nakaya HI, Fabro AT, Cunha TM, Alves-Filho JC, Zamboni DS, Cunha FQ. Gasdermin D inhibition prevents multiple organ dysfunction during sepsis by blocking NET formation. Blood. 2021. Epub 2021/08/19. doi: 10.1182/blood.2021011525. PubMed PMID: 34407544.
32. Zhang Y, Zhang R, Han X. Disulfiram inhibits inflammation and fibrosis in a rat unilateral ureteral obstruction model by inhibiting gasdermin D cleavage and pyroptosis. Inflamm Res. 2021;70(5):543-52. Epub 2021/04/15. doi: 10.1007/s00011-021-01457-y. PubMed PMID: 33851234.
33. Zhang Y, Cui J, Zhang G, Wu C, Abdel-Latif A, Smyth SS, Shiroishi T, Mackman N, Wei Y, Tao M, Li Z. Inflammasome activation promotes venous thrombosis through pyroptosis. Blood Adv. 2021;5(12):2619-23. Epub 2021/06/22. doi: 10.1182/bloodadvances.2020003041. PubMed PMID: 34152402; PMCID: PMC8270666.
34. Zhang Z, Zhang Y, Xia S, Kong Q, Li S, Liu X, Junqueira C, Meza-Sosa KF, Mok TMY, Ansara J, Sengupta S, Yao Y, Wu H, Lieberman J. Gasdermin E suppresses tumour growth by activating anti-tumour immunity. Nature. 2020;579(7799):415-20. Epub 2020/03/20. doi: 10.1038/s41586-020-2071-9. PubMed PMID: 32188940; PMCID: PMC7123794.
35. Wang C, Yang T, Xiao J, Xu C, Alippe Y, Sun K, Kanneganti TD, Monahan JB, Abu-Amer Y, Lieberman J, Mbalaviele G. NLRP3 inflammasome activation triggers gasdermin D-independent inflammation. Sci Immunol. 2021;6(64):eabj3859. Epub 2021/10/23. doi: 10.1126/sciimmunol.abj3859. PubMed PMID: 34678046.
36. Zhou Z, He H, Wang K, Shi X, Wang Y, Su Y, Wang Y, Li D, Liu W, Zhang Y, Shen L, Han W, Shen L, Ding J, Shao F. Granzyme A from cytotoxic lymphocytes cleaves GSDMB to trigger pyroptosis in target cells. Science. 2020;368(6494). Epub 2020/04/18. doi: 10.1126/science.aaz7548. PubMed PMID: 32299851.
37. Xia W, Li Y, Wu M, Jin Q, Wang Q, Li S, Huang S, Zhang A, Zhang Y, Jia Z. Gasdermin E deficiency attenuates acute kidney injury by inhibiting pyroptosis and inflammation. Cell Death Dis. 2021;12(2):139. Epub 2021/02/06. doi: 10.1038/s41419-021-03431-2. PubMed PMID: 33542198; PMCID: PMC7862699.
38. Aizawa E, Karasawa T, Watanabe S, Komada T, Kimura H, Kamata R, Ito H, Hishida E, Yamada N, Kasahara T, Mori Y, Takahashi M. GSDME-Dependent Incomplete Pyroptosis Permits Selective IL-1alpha Release under Caspase-1 Inhibition. iScience. 2020;23(5):101070. Epub 2020/05/04. doi: 10.1016/j.isci.2020.101070. PubMed PMID: 32361594; PMCID: PMC7200307.
39. Liu Y, Fang Y, Chen X, Wang Z, Liang X, Zhang T, Liu M, Zhou N, Lv J, Tang K, Xie J, Gao Y, Cheng F, Zhou Y, Zhang Z, Hu Y, Zhang X, Gao Q, Zhang Y, Huang B. Gasdermin E-

mediated target cell pyroptosis by CAR T cells triggers cytokine release syndrome. Sci Immunol. 2020;5(43). Epub 2020/01/19. doi: 10.1126/sciimmunol.aax7969. PubMed PMID: 31953257.
40. Chen KW, Demarco B, Ramos S, Heilig R, Goris M, Grayczyk JP, Assenmacher CA, Radaelli E, Joannas LD, Henao-Mejia J, Tacchini-Cottier F, Brodsky IE, Broz P. RIPK1 activates distinct gasdermins in macrophages and neutrophils upon pathogen blockade of innate immune signaling. Proc Natl Acad Sci U S A. 2021;118(28). Epub 2021/07/15. doi: 10.1073/pnas.2101189118. PubMed PMID: 34260403; PMCID: PMC8285957.
41. Ying J, Xu T, Wang C, Jin H, Tong P, Guan J, Abu-Amer Y, O'Keefe R, Shen J. Dnmt3b ablation impairs fracture repair through upregulation of Notch pathway. JCI insight. 2020;5(3). Epub 2020/02/14. doi: 10.1172/jci.insight.131816. PubMed PMID: 32051335; PMCID: PMC7098799.
42. Takeshita S, Kaji K, Kudo A. Identification and characterization of the new osteoclast progenitor with macrophage phenotypes being able to differentiate into mature osteoclasts. J Bone Miner Res. 2000;15(8):1477-88. Epub 2000/08/10. doi: 10.1359/jbmr.2000.15.8.1477. PubMed PMID: 10934646.
43. Wang C, Hockerman S, Jacobsen EJ, Alippe Y, Selness SR, Hope HR, Hirsch JL, Mnich SJ, Saabye MJ, Hood WF, Bonar SL, Abu-Amer Y, Haimovich A, Hoffman HM, Monahan JB, Mbalaviele G. Selective inhibition of the p38α MAPK-MK2 axis inhibits inflammatory cues including inflammasome priming signals. J Exp Med. 2018;215(5):1315-25. Epub 2018/03/20. doi: 10.1084/jem.20172063. PubMed PMID: 29549113; PMCID: PMC5940269.
44. Marsell R, Einhorn TA. The biology of fracture healing. Injury. 2011;42(6):551-5. Epub 2011/04/15. doi: 10.1016/j.injury.2011.03.031. PubMed PMID: 21489527; PMCID: PMC3105171.
45. Zhu H, Zhao M, Chang C, Chan V, Lu Q, Wu H. The complex role of AIM2 in autoimmune diseases and cancers. Immun Inflamm Dis. 2021;9(3):649-65. Epub 2021/05/21. doi: 10.1002/iid3.443. PubMed PMID: 34014039; PMCID: PMC8342223.
46. Yang C, Lei L, Collins JWM, Briones M, Ma L, Sturdevant GL, Su H, Kashyap AK, Dorward D, Bock KW, Moore IN, Bonner C, Chen CY, Martens CA, Ricklefs S, Yamamoto M, Takeda K, Iwakura Y, McClarty G, Caldwell HD. Chlamydia evasion of neutrophil host defense results in NLRP3 dependent myeloid-mediated sterile inflammation through the purinergic P2X7 receptor. Nat Commun. 2021;12(1):5454. Epub 2021/09/17. doi: 10.1038/s41467-021-25749-3. PubMed PMID: 34526512; PMCID: PMC8443728.
47. Zhang T, Tsutsuki H, Islam W, Ono K, Takeda K, Akaike T, Sawa T. ATP exposure stimulates glutathione efflux as a necessary switch for NLRP3 inflammasome activation. Redox Biol. 2021;41:101930. Epub 2021/03/20. doi: 10.1016/j.redox.2021.101930. PubMed PMID: 33740502; PMCID: PMC7995658.
48. Mbalaviele G, Novack DV, Schett G, Teitelbaum SL. Inflammatory osteolysis: a conspiracy against bone. J Clin Invest. 2017;127(6):2030-9. Epub 2017/06/02. doi: 10.1172/JCI93356. PubMed PMID: 28569732; PMCID: PMC5451216.
49. Novack DV, Mbalaviele G. Osteoclasts-Key Players in Skeletal Health and Disease. Microbiol Spectr. 2016;4(3). Epub 2016/06/24. doi: 10.1128/microbiolspec.MCHD-0011-2015. PubMed PMID: 27337470; PMCID: PMC4920143.
50. Nystrom S, Antoine DJ, Lundback P, Lock JG, Nita AF, Hogstrand K, Grandien A, Erlandsson-Harris H, Andersson U, Applequist SE. TLR activation regulates damage-associated molecular pattern isoforms released during pyroptosis. EMBO J. 2013;32(1):86-99. Epub 2012/12/12. doi: 10.1038/emboj.2012.328. PubMed PMID: 23222484; PMCID: PMC3545309.
51. Kitazawa R, Kimble RB, Vannice JL, Kung VT, Pacifici R. Interleukin-1 receptor antagonist and tumor necrosis factor binding protein decrease osteoclast formation and bone resorption in ovariectomized mice. J Clin Invest. 1994;94(6):2397-406. Epub 1994/12/01. doi: 10.1172/JCI117606. PubMed PMID: 7989596; PMCID: PMC330070.
52. Buettmann EG, McKenzie JA, Migotsky N, Sykes DA, Hu P, Yoneda S, Silva MJ. VEGFA From Early Osteoblast Lineage Cells (Osterix+) Is Required in Mice for Fracture Healing. J Bone

Miner Res. 2019;34(9):1690-706. Epub 2019/05/14. doi: 10.1002/jbmr.3755. PubMed PMID: 31081125; PMCID: PMC6744295.

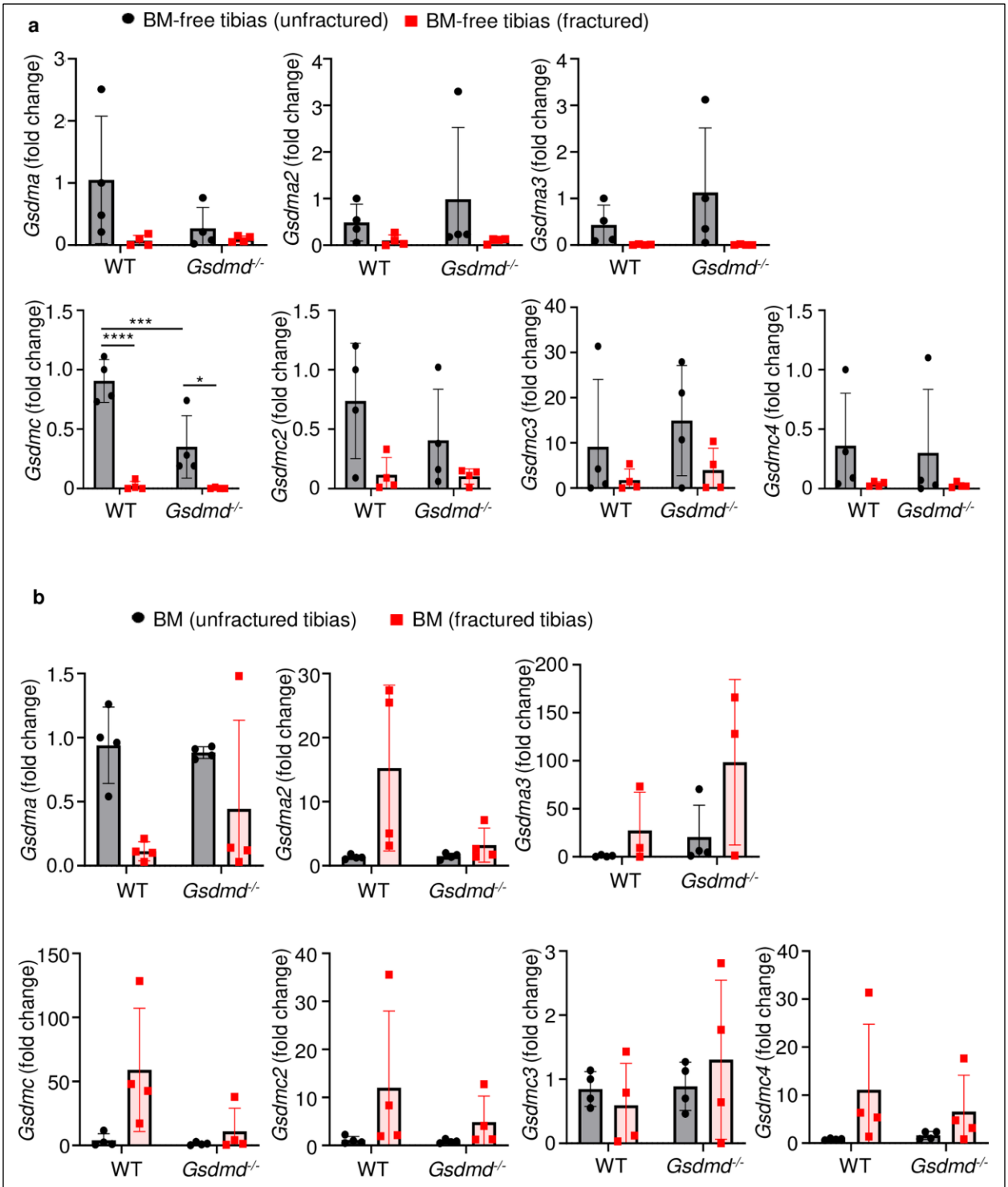

Fig. S1. **S**everal GSDM family members were barely expressed in bones. RNAs were isolated from BM-free bones (**a**) or BM (**b**) were from 12-week-old male WT or *Gsdmd*$^{-/-}$ mice (n=4-5). Samples were isolated from unfractured or fractured tibias (3 days after injury). qPCR (**a**, **b**) analysis. Data were normalized to unfractured WT, and were mean ± SD. *P < 0.05; ***P < 0.001; ****P < 0.0001, two-way ANOVA with Tukey's multiple comparisons test.

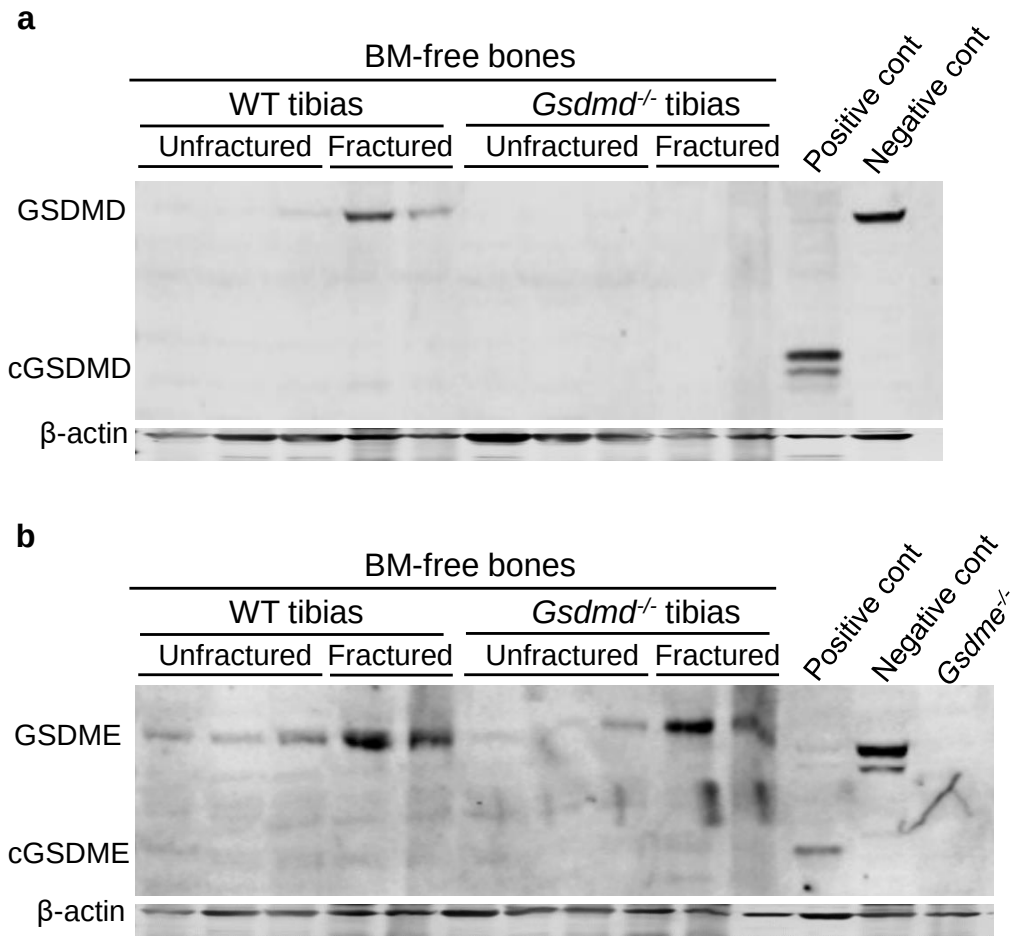

Fig. S2. Fracture induced GSDMD and GSDME expression. Proteins were isolated from BM-free tibias from 12-week-old male WT or *Gsdmd*$^{-/-}$ mice. Tibias were unfractured or fractured (3 days after injury). GSDMD (**a**) and GSDME (**b**) were analyzed by immunoblotting. cGSDMD, cleaved GSDMD; cGSDME, cleaved GSDME; WT, wild-type.

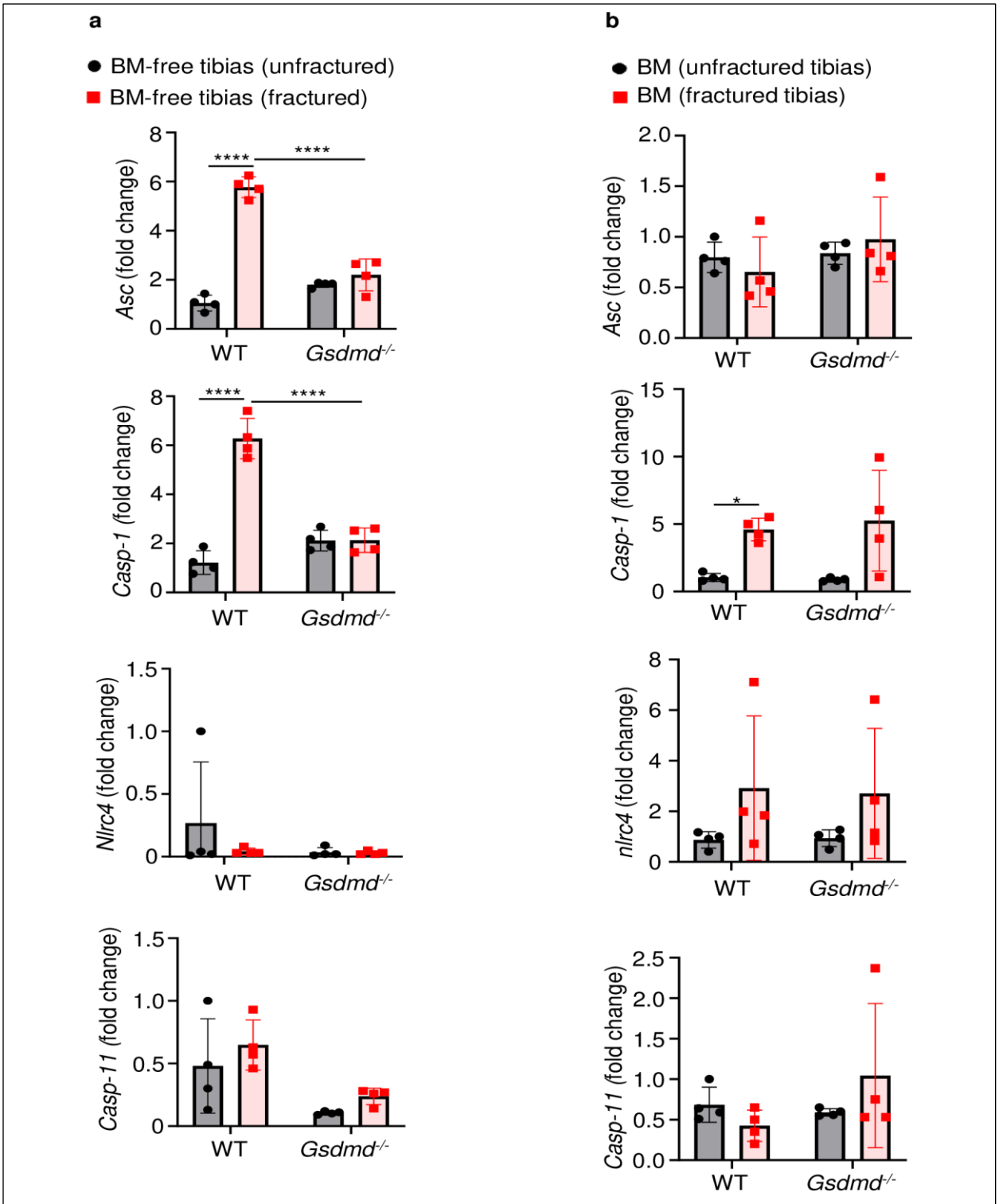

Fig. S3. Fracture induced the expression of certain inflammasome components. RNAs were isolated from BM-free bones (**a**) or BM (**b**) were from 12-week-old male WT or *Gsdmd*$^{-/-}$ mice (n=4). Tibias were unfractured or fractured (3 days after injury). RNAs were analyzed by qPCR. Data were normalized to unfractured WT, and were mean ± SD *P < 0.05; ***P < 0.001; ****P < 0.0001, two-way ANOVA with Tukey's multiple comparisons test. WT, wild-type.

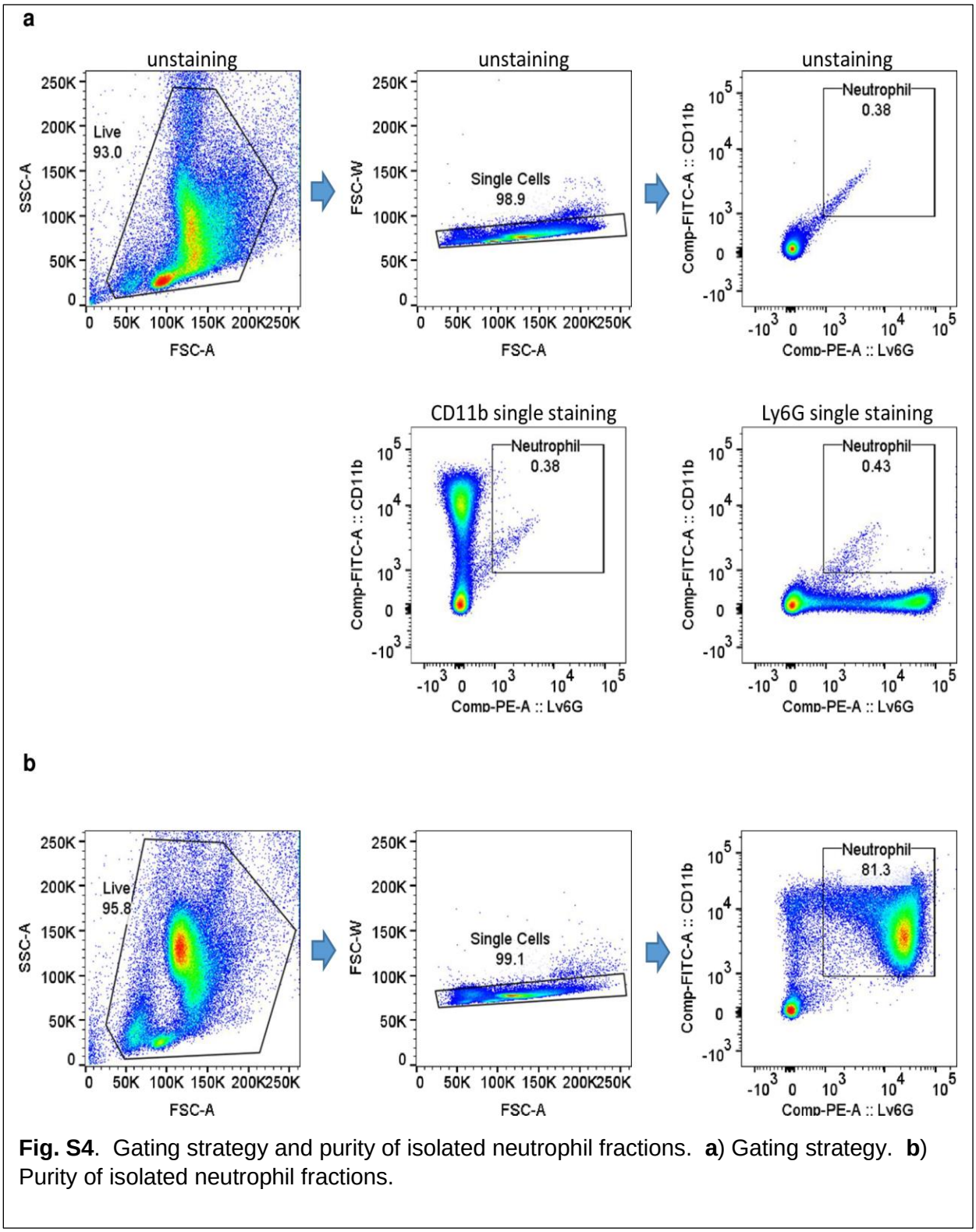

Fig. S4. Gating strategy and purity of isolated neutrophil fractions. **a**) Gating strategy. **b**) Purity of isolated neutrophil fractions.

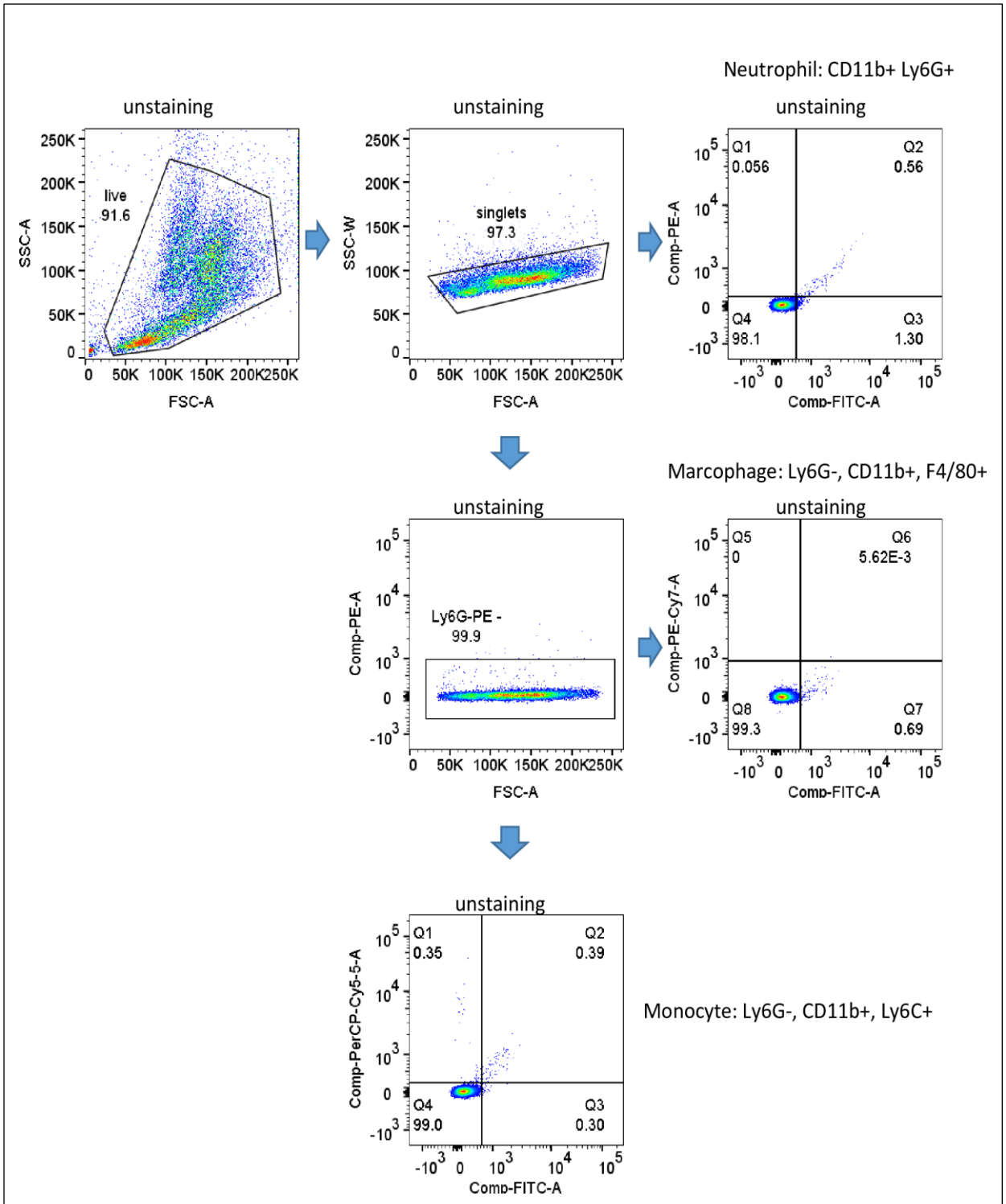

Fig. S5. Gating strategy for **Fig. 5a-c.**

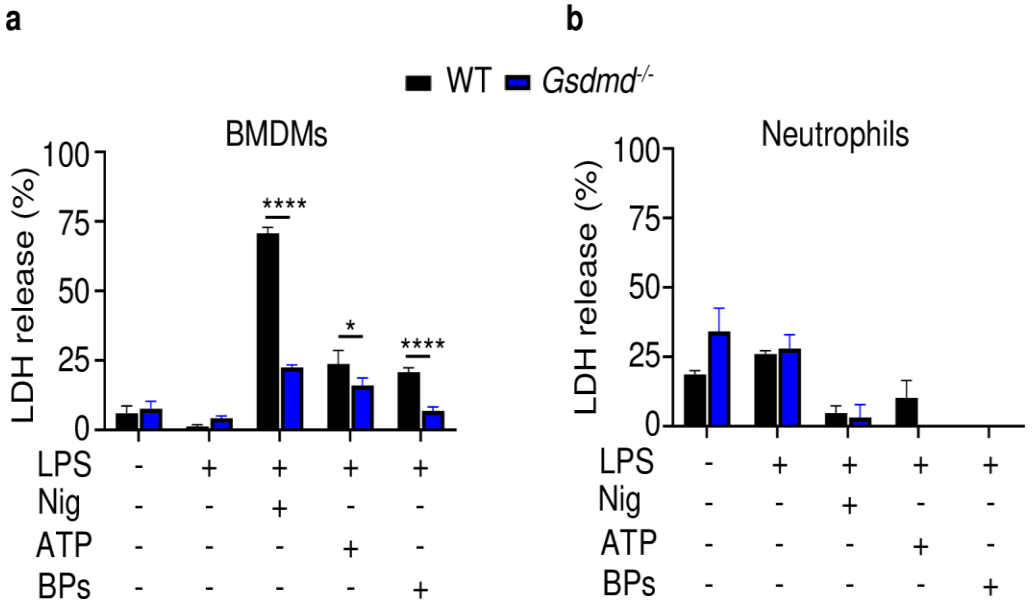

Fig. S6. Effects of GSDMD loss on LDH release. Bone marrow cells were isolated from 12-week-old male WT or *Gsdmd*$^{-/-}$ mice. BMDMs (**a**) were expanded *in vitro* whereas neutrophils (**b**) were used immediately after purification. Cells were primed with 100 ng/ml LPS for 3 hours, then with 15 μM nigericin for 1 hour, 5 mM ATP for 1 hour, or 50 mg/ml bone particles for 2 hours. LDH was measured in conditioned medium. Data are mean ± SD of triplicates and were representative of at least three independent experiments. *P < 0.05; ****P < 0.0001, two-way ANOVA with Tukey's multiple comparisons test. BPs, bone particles; LDH, lactate dehydrogenase; WT, wild-type.